Anomalous stress-strain behavior of NiTi shape memory alloy close to the border of superelastic window

Graphical Abstract

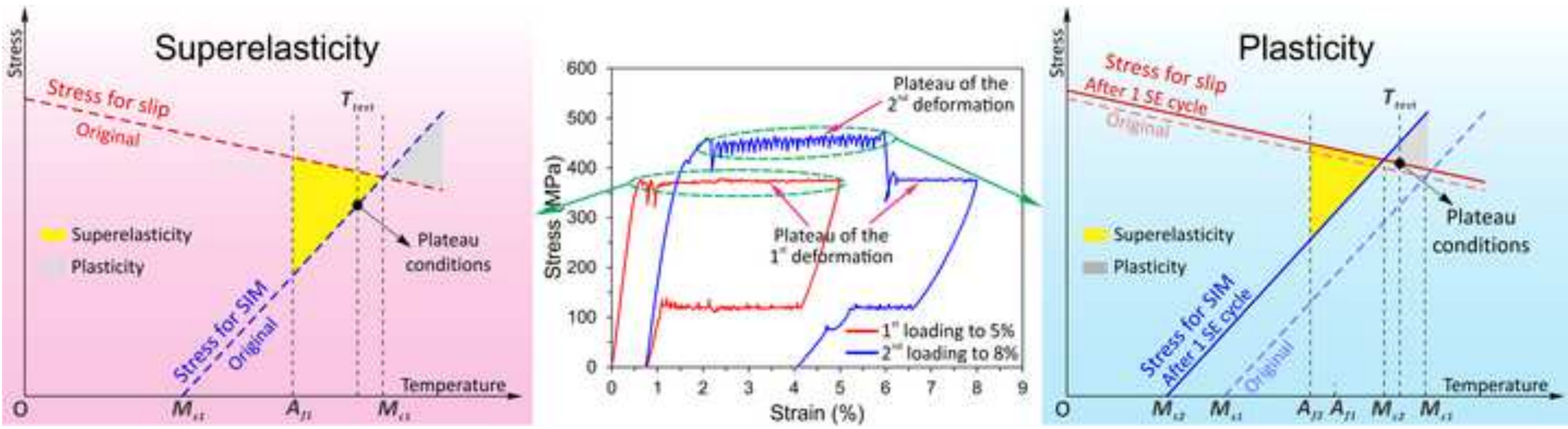

Anomalous stress-strain behavior of NiTi shape memory alloy close to the border of superelastic window

Xiebin Wang[a,b,*], Xiayang Yao[c], Dominique Schryvers[c], Bert Verlinden[d], Guilong Wang[a], Guoqun Zhao[a], Jan Van Humbeeck[d], Sergey Kustov[e]

[a]Key Laboratory for Liquid-Solid Structural Evolution and Processing of Materials (Ministry of Education), Shandong University, Jingshi Road 17923, Jinan 250061, China.

[b]Suzhou Institute of Shandong University, Ruoshui Road 388, Suzhou 215123, China.

[c]Electron Microscopy for Materials Science (EMAT), University of Antwerp, Groenenborgerlaan 171, Antwerp B-2020, Belgium.

[d]Department of Materials Engineering, University of Leuven (KU Leuven), Kasteelpark Arenberg 44 bus 2450, Heverlee B-3001, Belgium.

[e]Departament de Física, Universitat de les Illes Balears, Cra Valldemossa km 7.5, Palma de Mallorca E07122, Spain.

*Corresponding author: xiebin.wang@email.sdu.edu.cn, wangxiebin@sdu.edu.cn (X. Wang)

Abstract

In this work, we report an anomalous phenomenon on superelastic cycling of NiTi shape memory alloys when deforming at the temperature close to the border of superelastic window. New unexpected effects are found: (*i*) critical stress for inducing martensite transformation during the second loading cycle is higher than that of the first cycle; (*ii*) the plateau stress of the second cycle decreases to the original level when the strain overcomes the limit of the first cycle; (*iii*) transition from good superelasticity in the first cycle to fully irreversible strain in the second. We propose that defects generated during the first superelastic cycle close to the border of superelastic window impede following stress-induced martensitic transformations, leading to the increase of critical stress beyond yield stress of the B2 matrix, and thus functional fatigue of NiTi alloys.

Keywords: Shape memory alloy, NiTi, Plastic deformation, Superelasticity, Functional fatigue.

Near equiatomic NiTi shape memory alloy transforms thermoelastically between a B2 structured austenite (A) and B19' martensite (M), giving rise to the effects of shape memory and superelasticity [1], which are widely employed in practical applications [2,3]. Apart from the unique functional properties, the mechanism of plastic deformation in NiTi alloys has attracted increasing interest [4-10], since plastic activities accompanying the martensitic transformation (MT) are the main reason for the functional degradation of NiTi alloys [10-14]. Thus, understanding the origin of these plastic activities is a key step to improve the functional stability of NiTi alloys.

The origin of the plastic activities accompanying the MT in NiTi has been studied both through experimental work and simulation [4-6]. Because the B2 and B19' phases have different lattice structure [1], the strain compatibility of the coherent A/M interface during transformation has been addressed. It is suggested that, in order to accommodate the local strain gradient, plastic slip during the forward A→M transformation may occur either at the A/M interface [7,15,16], or in the austenite [10,12,16-21] / martensite [9,22] matrix adjacent to the A/M interface. The dislocation slip occurring during the reverse transformation is also discussed [16-18,23]. Deformation twinning is another possible contribution of the irreversible strain [8,24-28], especially when deforming at elevated temperatures [8] or subjected to high loading cycles [25].

However, to the best of our knowledge, the origin of plastic activities in NiTi alloys during stress-induced MT is still ambiguous, mainly due to the complexity of this process, involving phase transformation, dislocation slip, martensite twin migration, and deformation twinning. Moreover, the deformation behavior of NiTi is sensitive to many other factors, for instance, crystallographic orientation and texture [29-31], presence of inclusions or precipitates [32-34], grain size [35,36], thermo-mechanical history (e.g., post-deformation annealing, aging) [37,38], load path [39,40], strain rate [41-43], strain amplitude [8], and testing temperature [5,23]. The experimental work with unconventional deformation behavior might help to understand the plastic deformation in NiTi alloys, as previously suggested by Chen *et al.* [8].

In the present work, following this idea, we study superelastic behavior of NiTi upon approaching the border of superelastic window in order to study the transition from superelastic to plastic deformation. We show that the role of defects created during stress-induced MT changes close to this border, and the effect should be taken into account in functional fatigue of NiTi alloys.

A cold drawn Ti-50.8 at.% Ni wire of 100 μm diameter (Memory-Metalle GmbH, Germany) was used. The as-received wire was annealed for 30 min at different temperatures (773, 823 and 873 K) under protective Ar atmosphere and water-quenched at room temperature. Major attention was paid to 873 K-annealed samples, while the 773 K and 823 K-annealed ones served as a reference. The 873 K-annealed sample shows a direct MT start temperature (M_s) at 227 K and reverse MT finish temperature (A_f) at 257 K (Fig. S1 in supplement). Mechanical tests were carried out using a TA Q800 dynamic mechanical analyzer under a constant strain rate of 1.67×10^{-4} s^{-1}. Electrical resistance (ER) measurements were performed to characterize the transformation behavior. The resistivity was registered using AC excitation and lock-in detection in a home-made four-probe measuring system under a cooling/heating rate of 2 K min^{-1}. The microstructure was investigated by means of electron backscatter diffraction (EBSD) and transmission electron microcopy (TEM). EBSD tests were performed using a TSL/EDAX system on a FEI Nova NanoSEM 450 microscope. For EBSD observations, the surface parallel to the wire axis was prepared using a JEOL IB-09010CP cross-section polisher. TEM was conducted using a FEI Tecnai G2 microscope operated at 200 kV. The TEM foils, taken along the wire axis, were prepared by focused ion beam (FIB) with the 'lift-out' procedure in a FEI Helios 650 NanoLab SEM/FIB instrument, an example of the TEM sample is shown in Fig. S2 in supplement.

Figure 1a shows typical reference superelastic stress-strain curves in two consecutive cycles for an 823 K-annealed sample. As the stress reaches a critical value, the stress-induced martensite transformation (SIMT) occurs through a Lüders-like mechanism [44,45], giving rise to a stress plateau during loading. Except for a small amount of residual strain, most of the strain is recovered during unloading due to the reverse M→A transformation, which also produces a stress plateau. The residual strain is mainly caused by the plastic activities associated with the forward and/or reverse transformation [4-6]. These plastic activities induce an internal stress field, which can assist the formation of martensite variants [15,19,46] in consecutive SIMTs. As a result, the critical stress of SIMT is lower in the second cycle than in the first cycle (blue curve in Fig. 1a), but only for the strain below the maximum reached in the first cycle. The critical stress ***increases to the original level*** as soon as the strain exceeds the limit of the first cycle. A relatively small increase of irrecoverable strain (around 0.5%) is observed after the second cycle.

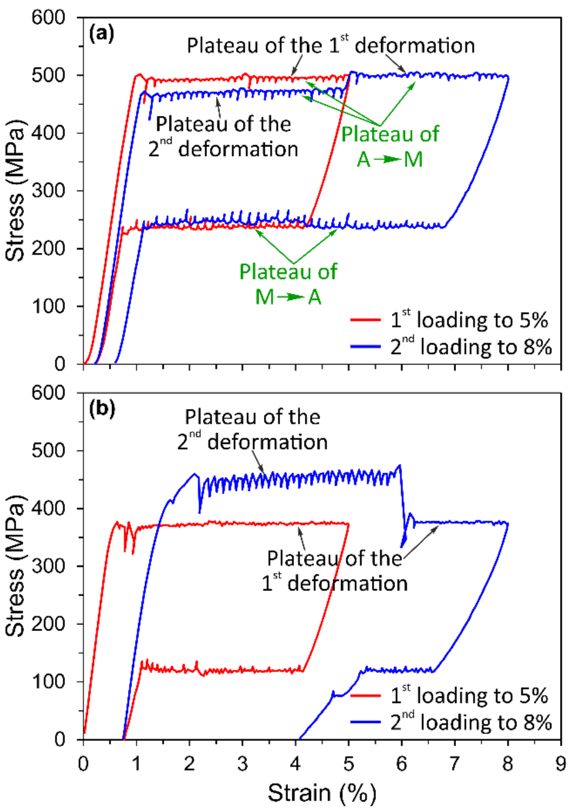

Figure 1. Stress-strain curves of a cold-drawn Ti-50.8 at.% wire after annealing for 30 min at (a) 823 K, and (b) 873 K. The samples are loaded at 298 K to a strain of 5% and 8% during the first and second cycle, respectively.

Figure 1b shows the cyclic deformation behavior of the 873 K-annealed sample. The results exemplify the unusual stress-strain behavior at 298 K, and the striking observations are: (*i*) the plateau stress of the second cycle is higher than that of the first cycle, which is different from the conventional superelastic behavior (Fig. 1a); (*ii*) opposite to the behavior of the 823 K-annealed sample (Fig. 1a), the plateau stress ***drops to the original level*** of the first cycle, when the strain exceeds the limit of the first cycle. Thus, in the second loading cycle, in violation of the expected natural sequence, the deformation proceeds first at a high stress and then at a substantially lower one (Fig. 1b blue curve, and Fig. S3 in supplement); (*iii*) the first cycle shows good superelasticity, but the second one shows recoverable strain comparable only with the strain added in the second cycle (Fig. 1b and Fig. S4 in supplement). The strain around 4.3% that was essentially reversible (superelasticity) in the first cycle becomes irreversible in second cycle. Incremental loading-unloading cycles up to a strain of 25% (Fig. S5 in supplement), indicate that these unusual features persist in consecutive cycles until the strain becomes purely plastic.

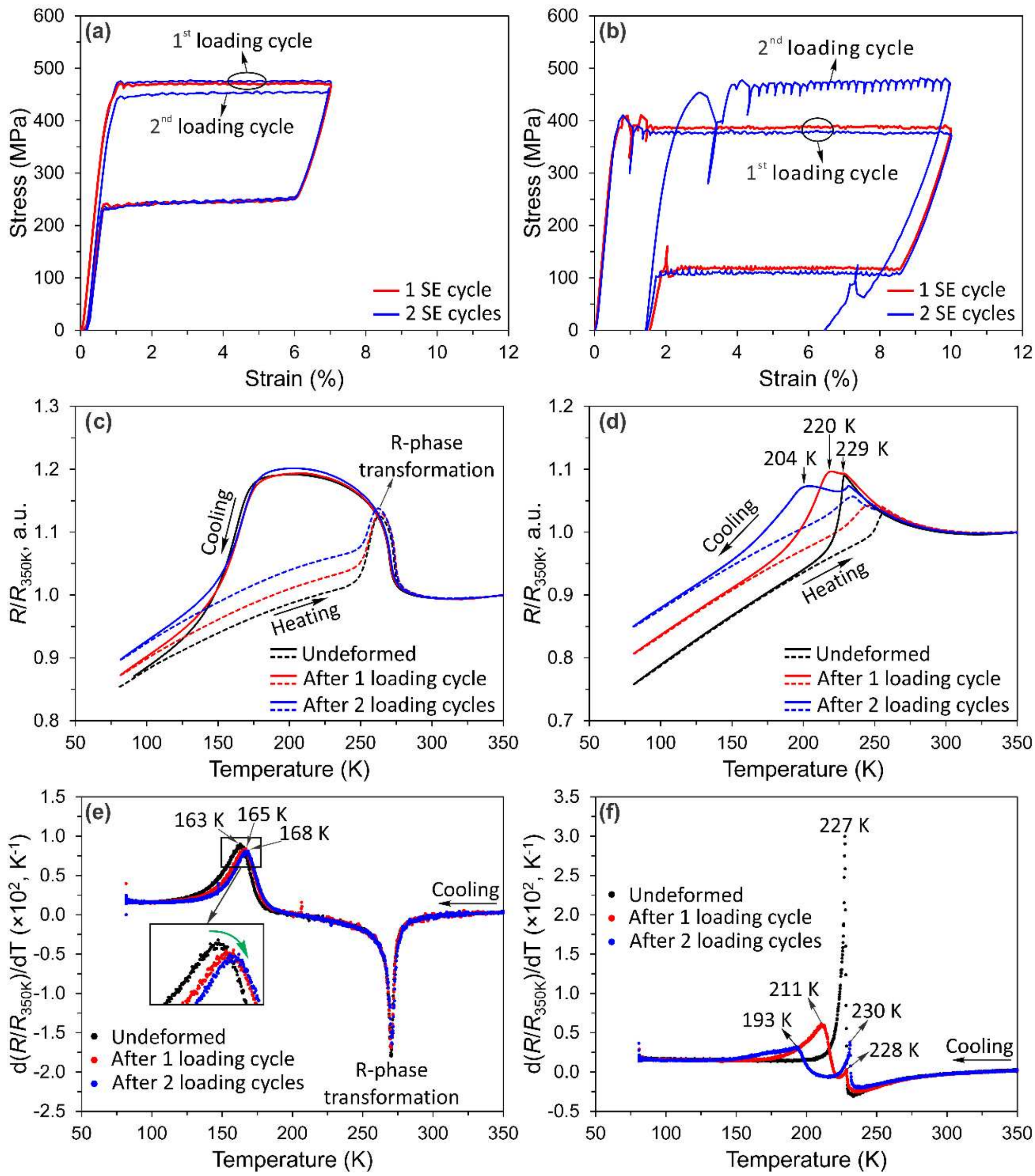

Figure 2. Stress-strain curves of a cold drawn Ti-50.8 at.% Ni wire after annealing for 30 min at (a) 773 K and (b) 873 K. Two samples were subjected to tensile loading-unloading tests at 298 K for 1 and 2 cycles, respectively. The electric resistance curves of (c) the 773K-annealed and (d) the 873K-annealed samples before and after one and two loading cycles. (e) and (f) show temperature derivative of the electrical resistance from (c) and (d), respectively.

Figure 2 shows the preparatory stress-strain cycles for cold drawn Ti-50.8 at.% Ni wire after annealing at 773 (a) and 873 K (b). The sample annealed at 773 K shows a conventional superelastic response, as frequently reported in literature [1,47], while the one annealed at 873 K shows the abovementioned counterintuitive behavior. The influence of superelastic loading on the temperature-induced MT was characterized by ER measurements. According to Ref. [48], dR/dT perfectly correlates with the transformation rate in NiTi alloys. Resistivity measurements detect at around 270 K well documented the R-phase transformation in the 773 K-annealed sample (Fig. 2c), which is due to the incomplete annealing and formation of coherent Ni_4Ti_3 precipitates during annealing below 873 K [1,47,49]. On further cooling the R-phase transforms into martensite at around 160 K. The R-phase to martensite transformation shifts gradually to higher temperatures upon superelastic cycling (Fig. 2e). The dR/dT peak temperature is 163 K for the as-annealed state, shifting to 165 K and to 168 K after one and two superelastic cycles, respectively. The increase of transformation temperature is consistent with the decrease of the plateau stress, according to the Clausius-Clapeyron type relation [1]. It has frequently been suggested that a “directional” internal stress field could be generated after superelastic loading, due to the plastic activities associated with SIMT [15,19,30,46]. The stress field can promote the MT and thus leads to the decrease of the plateau stress (Fig. 2a) and increase of the transformation temperatures (Fig. 2c and 2e) after superelastic cycling.

Figures 2d and 2f show the R(T) and its temperature derivative for the 873 K-annealed sample, also in as annealed state and after 1 and 2 superelastic cycles (Fig. 2b). The R-phase transformation is absent, due to the full annealing of the cold-worked microstructure at 873 K [37,50,51]. A remarkable observation is the strong splitting of the direct MT into two stages in deformed samples. The temperature of the first step in deformed samples is the same as in the as-annealed state. Therefore, the two steps of the MT in deformed samples should be associated with parts of the material that suffered the SIMT and remained not transformed. Crucial observation is that the second step of the MT, related with the part of the sample that suffered SIMT, is strongly shifted to lower temperatures by 16 and 34 K after one and two loading cycles, respectively (Fig. 2f). The decrease of the MT temperature is also revealed by DSC measurement (Fig. S6 in supplement). Thus, the effect of SIMT during cyclic loading on temperature-induced MT is opposite in samples annealed at 773 and 873 K, pointing to the different status of defects generated during superelastic cycling.

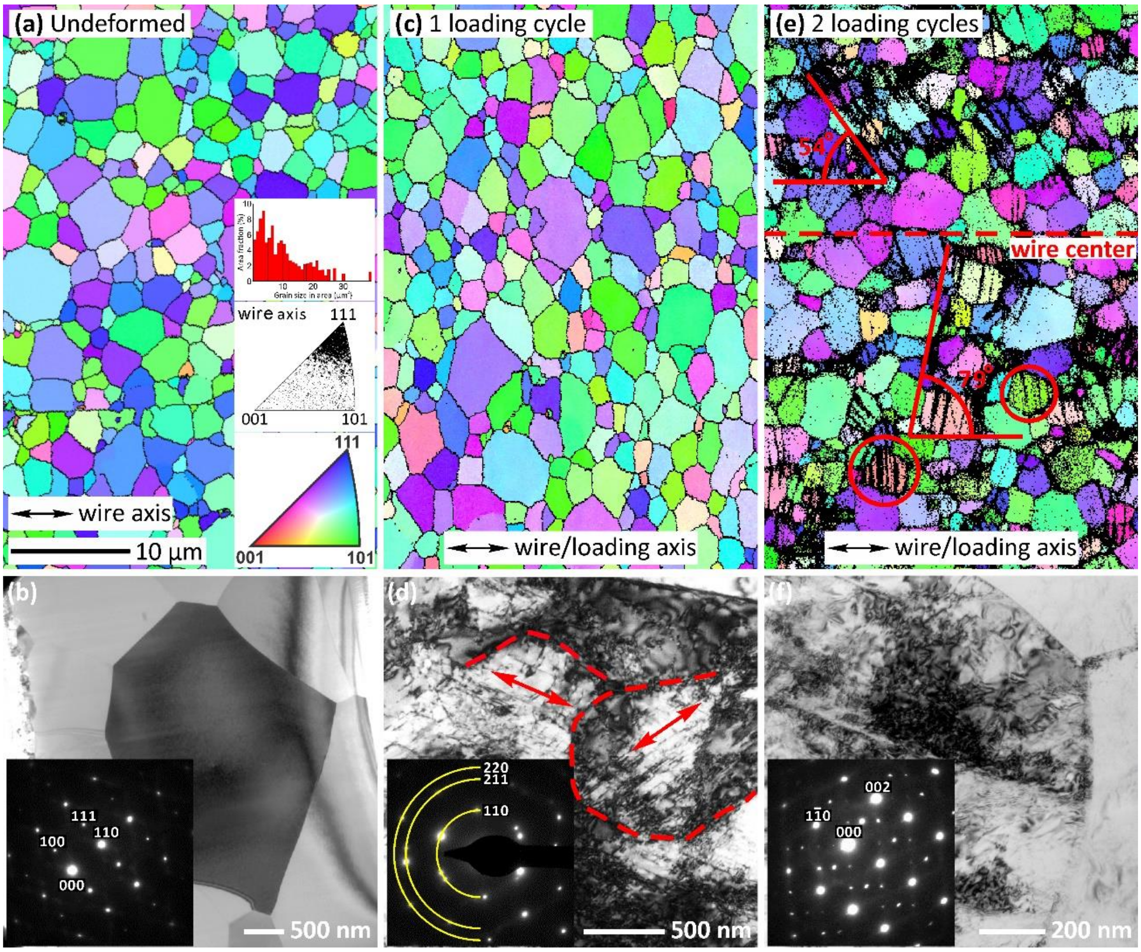

Figure 3. (a) EBSD orientation map and (b) TEM bright field image of a cold drawn Ti-50.8 at.% Ni wire after annealing at 873 K for 30 min. The grain size distribution chart, inverse pole figure with respect to the wire axis, and the color code are inserted in (a). (c) EBSD map and (d) TEM bright filed image of the as-annealed sample after 1 loading-unloading cycle at 298 K. (e) EBSD map and (f) TEM bright field image of the as-annealed sample after 2 loading-unloading cycles at 298 K. The dash lines in (d) roughly indicate some grain boundaries.

Figure 3 shows the microstructure of the 873 K-annealed sample, which possesses the uncovered anomalous stress-strain behavior (Fig. 1b). The EBSD map of as-annealed sample in Fig. 3a shows a fully recrystallized microstructure with equiaxed grains. The average grain size was manually determined as 2.0 μm using the line intercept method described by Sutou *et al.* [52]. Figure 3a also gives the inverse pole figure with reference to the wire axis, and a strong <111>$_{B2}$ fiber texture is revealed. TEM observations (Fig. 3b) reveal very low dislocation density and sharp grain boundaries. The corresponding selected area diffraction (SAD) pattern in Fig. 3b confirms that the as-annealed sample is in B2 austenite phase at room temperature.

EBSD results for the sample after 1 superelastic cycle (Fig. 3c) do not show any obvious microstructural difference as compared with the as-annealed state (Fig. 3a). Nevertheless, a significant increase of dislocation density is revealed by TEM (Fig. 3d). The massive dislocation slip results in an irrecoverable strain of 1.4% after unloading (Fig. S7 in supplement). The dislocation network consists mainly of arrays, frequently reported after superelastic cycling [16-18,20]. The direction of dislocation arrays, as marked by the arrows in Fig. 3d, varies in different grains, confirming a strong influence of crystallographic orientation [16-18,20,53].

After 2 superelastic cycles, EBSD reveals massive traces of plastic deformation (Fig. 3e). The deformation bands are inclined clockwise and counterclockwise with respect to the wire axis below and above the wire axis, respectively. This feature points to the formation of a cone-shaped A/M interface during SIMT in the wire, as reported by Sedmark *et al.* [54]. Unlike the frequently reported inclination angle around 55° for the macroscopic Lüders bands [21,55], the inclination angle of the deformation bands in Fig. 3e varies largely over different grains. TEM observations (Fig. 3f) reveal a high density of entangled dislocations. Straight dislocation segments are not observed, in contrast to the sample subjected to 1 superelastic cycle.

Figure 4 shows the cyclic stress-strain response of 873 K-annealed samples tested at different temperatures. It indicates that the appearance of the counterintuitive phenomenon depends highly on the testing temperature. The superelasticity is absent when testing at 228 and 273 K, because the low testing temperature prohibits the reverse transformation. Superelasticity is observed when testing at and above 283 K. The plateau stress of both the first and second loading cycle increases with the increase of testing temperature. However, the plateau stress of the second cycle increases faster than that of the first cycle. The sample tested at 283 K shows a conventional superelastic response (Fig. 4c). At 285 K the two loading cycles show similar plateau stress (Fig. 4d). The uncovered unusual behavior is observed for tests between 288 and 303 K (Fig. 4e-4g). The sample loses completely superelasticity and undergoes plastic deformation at 313 K (Fig. 4i). Thus, this temperature is considered as the upper limit of the superelastic window for 873 K-annealed samples.

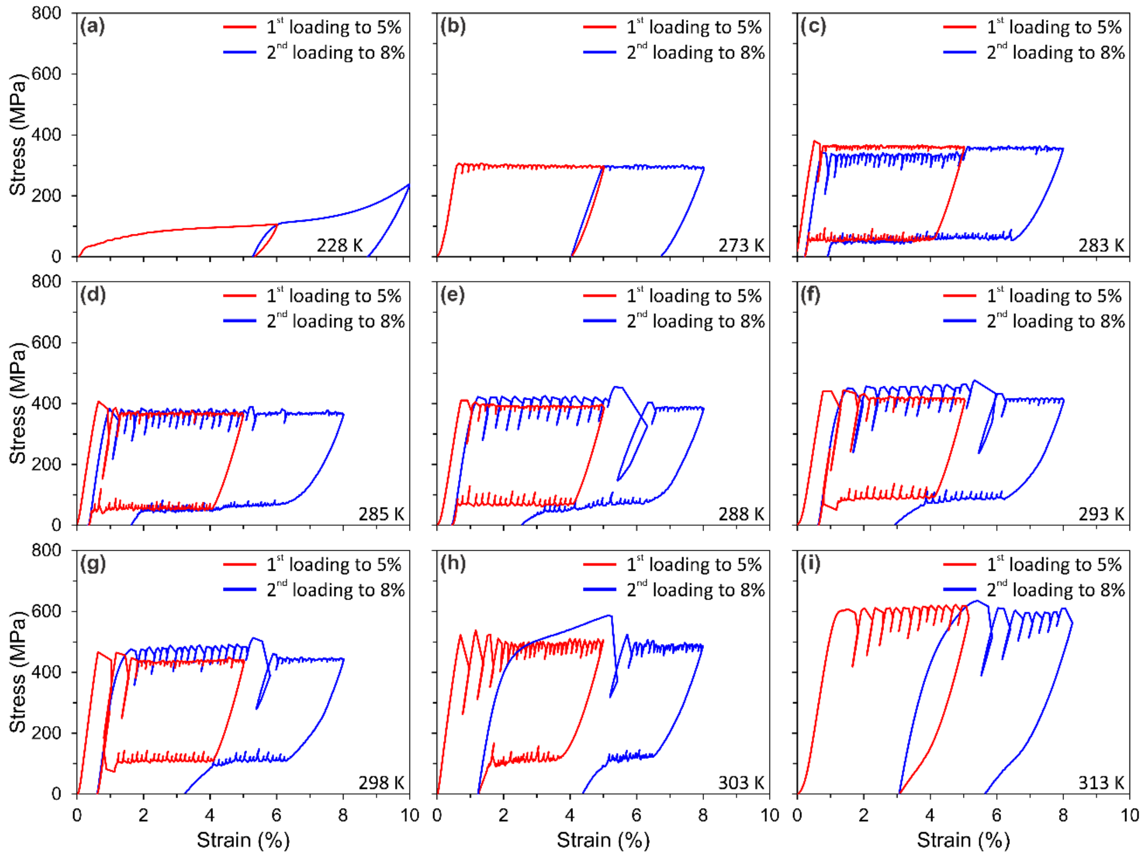

Figure 4. The stress-strain curves, tested at different temperatures, of a cold drawn Ti-50.8 at.% Ni wire after annealing at 873 K for 30 min.

Figure 5 explains a possible scenario that explains the occurrence of the anomalous stress-strain behavior just below the high-temperature border of the superelastic window (288-303 K in this work). Figure 5a illustrates the states of the material before the first loading cycle. With the increase of temperature, the critical stress for SIMT increases according to the Clausius-Clapeyron type relation, while the yield strength of the alloy decreases. Hence, we could define a critical temperature M_{c1}, at which the yield stress equals the stress for SIMT. The sample will lose superelasticity above M_{c1}, since plastic deformation will occur at a lower stress than SIMT. According to the results in Fig. 4, the testing temperature of 298 K is below but rather close to the M_{c1} temperature, since the sample loses superelasticity between 303 and 313 K.

The defects generated during the first superelastic cycle alter the state of the material, provoking the decrease of MT temperature (Fig. 2 and Fig. S5) from M_{s1} to M_{s2}. Therefore, the M_c temperature decreases to a lower value, M_{c2}, as is illustrated in Fig. 5b. Moreover, the critical stress for SIMT at fixed temperature of 298 K increases for the second loading cycle. Since the testing temperature is close to the high-temperature border of the superelastic window, the critical stress becomes higher than the yield stress of the austenite during the second cycle. That is, the testing temperature becomes higher than the modified M_{c2}. Therefore, the part of the sample that underwent SIMT in the first cycle undergoes plastic deformation during the second cycle. This interpretation leaves open the most intriguing question: why the SIMT of the “virgin” part of the sample occurs at lower stress ***after*** the plastic deformation of the transformed part during the second loading cycle (blue curve in Fig. 1b, and Fig. S3 in supplement)? Apparently, the simple interpretation based on Fig. 5 is not able to account for this counterintuitive behavior. Possible research line for the future work is to study the transformation interface during the first loading cycle, which might be the key to understand the uncovered effects. It is also worthy to check whether the reported effects are generic and inherent in other NiTi alloys (e.g. aged or partially annealed samples) at the temperatures close to the corresponding limit of superelastic window.

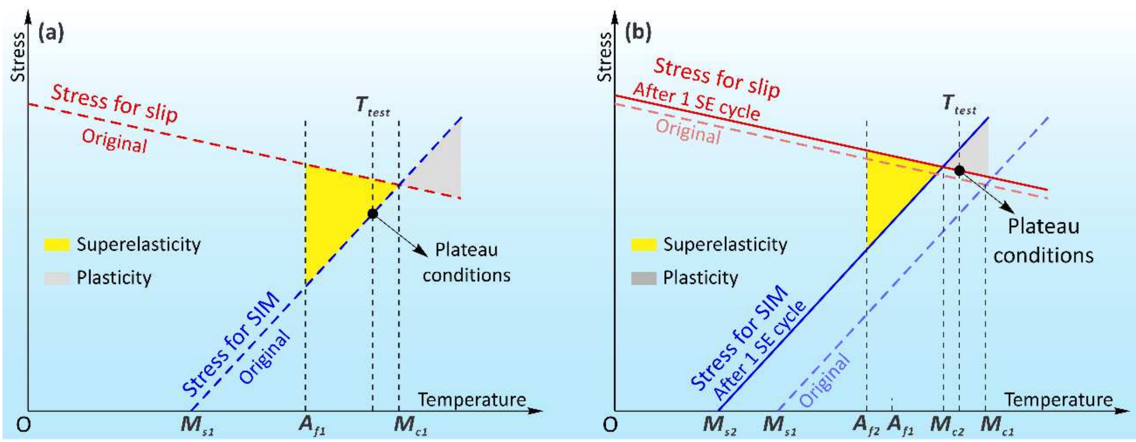

Figure 5. Schematic illustration of the states of the sample (a) before the first loading cycle, and (b) after the first loading cycle. M_c indicates the critical temperature, at which the critical stress for inducing martensite transformation (SIM) equals the yield stress of the matrix.

In summary, we argue that upon approaching the border of superelastic window, the role of defects created during stress-induced MT changes. Well below the limit of this window, the defects assist consecutive transformations through their stress fields. For stress-induced MT close to the limit of superelastic window, the created defects strongly impede consecutive MT. The change of the role of plastic activities upon approaching the border of superelastic window results in a transition from conventional superelasticity to the unusual stress-strain behavior with certain counterintuitive features. The different role of SIMT-induced defects, depending on the distance from the border of superelastic window, might be important in understanding and controlling functional fatigue of NiTi alloys.

Declaration of interests

The authors declare that they have no known competing financial interests or personal relationships that could have appeared to influence the work reported in this paper.

Acknowledgements

This work was supported by National Key R&D Program of China [grant number 2018YFB1105100]; National Nature Science Foundation of China [grant number 51905310]; Natural Science Foundation of Shandong Province [ZR2020YQ39]; Natural Science Foundation of Jiangsu Province [grant number BK20180231]; Key Research and Development Program of Shandong Province [grant number 2019GGX104065]; the Young Scholars Program of Shandong University [grant number 2018WLJH24]; and the Research Foundation Flanders [grant number G.0366.15N]. S. Kustov acknowledges the support from Spanish MCIU-AEI and FEDER, UE [project RTI 2018-094683-B-C51].

References

[1] K. Otsuka, X. Ren, Prog. Mater. Sci. 50 (2005) 511-678.

[2] C. Constant, S. Nichols, É. Wagnac, Y. Petit, A. Desrochers, V. Braïlovski, Materialia 9 (2020) 100567.

[3] D. Kapoor, Johnson Matthey Technol. Rev. 61 (2017) 66-76.

[4] P. Sittner, P. Sedlak, H. Seiner, P. Sedmak, J. Pilch, R. Delville, L. Heller, L. Kaderavek, Prog. Mater. Sci. 98 (2018) 249-298.

[5] P. Chowdhury, H. Sehitoglu, Prog. Mater. Sci. 85 (2017) 1-42.

[6] P. Chowdhury, H. Sehitoglu, Prog. Mater. Sci. 88 (2017) 49-88.

[7] H. Sehitoglu, Y. Wu, S. Alkan, E. Ertekin, Philos. Mag. Lett. 2017 (2017) 1-12.

[8] Y. Chen, O. Molnárová, O. Tyc, L. Kadeřávek, L. Heller, P. Šittner, Acta Mater. 180 (2019) 243-259.

[9] A.S.K. Mohammed, H. Sehitoglu, Acta Mater. 186 (2020) 50-67.

[10] H.M. Paranjape, M.L. Bowers, M.J. Mills, P.M. Anderson, Acta Mater. 132 (2017) 444-454.

[11] Y. Gao, Materialia 6 (2019).

[12] L. Heller, H. Seiner, P. Sittner, P. Sedlak, O. Tyc, L. Kaderavek, Int. J. Plast. 111 (2018) 53-71.

[13] Y. Gao, L. Casalena, M.L. Bowers, R.D. Noebe, M.J. Mills, Y. Wang, Acta Mater. 126 (2017) 389-400.

[14] W.-S. Ko, W.S. Choi, G. Xu, P.-P. Choi, Y. Ikeda, B. Grabowski, Acta Mater. 202 (2021) 331-349.

[15] P. Sedmak, P. Sittner, J. Pilch, C. Curfs, Acta Mater. 94 (2015) 257-270.

[16] T. Simon, A. Kröger, C. Somsen, A. Dlouhy, G. Eggeler, Acta Mater. 58 (2010) 1850-1860.

[17] D.M. Norfleet, P.M. Sarosi, S. Manchiraju, M.F.-X. Wagner, M.D. Uchic, P.M. Anderson, M.J. Mills, Acta Mater. 57 (2009) 3549-3561.

[18] M.L. Bowers, X. Chen, M. De Graef, P.M. Anderson, M.J. Mills, Scripta Mater. 78-79 (2014) 69-72.

[19] R.F. Hamilton, H. Sehitoglu, Y. Chumlyakov, H.J. Maier, Acta Mater. 52(11) (2004) 3383-3402.

[20] R. Delville, B. Malard, J. Pilch, P. Sittner, D. Schryvers, Acta Mater. 58 (2010) 4503-4515.

[21] H. Kato, K. Sasaki, Int. J. Plast. 50 (2013) 37-48.

[22] C. Yu, G. Kang, D. Song, Q. Kan, Int. J. Plast. 67 (2015) 69-101.

[23] L. Heller, P. Šittner, P. Sedlák, H. Seiner, O. Tyc, L. Kadeřávek, P. Sedmák, M. Vronka, Int. J. Plast. 116 (2019) 232-264.

[24] O. Benafan, R.D. Noebe, S.A. Padula, A. Garg, B. Clausen, S. Vogel, R. Vaidyanathan, Int. J. Plast. 51 (2013) 103-121.

[25] R. Delville, B. Malard, J. Pilch, P. Sittner, D. Schryvers, Int. J. Plast. 27 (2011) 282-297.

[26] T. Ezaz, H. Sehitoglu, H.J. Maier, Acta Mater. 60 (2012) 339-348.

[27] S. Ii, K. Yamauchi, Y. Maruhashi, M. Nishida, Scripta Mater. 49 (2003) 723-727.

[28] Y. Zhong, K. Gall, T. Zhu, Acta Mater. 60 (2012) 6301-6311.

[29] Z. Wang, J. Chen, C. Besnard, L. Kunčická, R. Kocich, A.M. Korsunsky, Acta Mater. 202 (2021) 135-148.

[30] A.W. Richards, R.A. Lebensohn, K. Bhattacharya, Acta Mater. 61 (2013) 4384-4397.

[31] C.P. Frick, B.G. Clark, A.S. Schneider, R. Maab, S. Van Petegem, H. Van Swygenhoven, Scripta Mater. 62 (2010) 492-495.

[32] P. Chowdhury, L. Patriarca, G. Ren, H. Sehitoglu, Int. J. Plast. 81 (2016) 152-167.

[33] M. Rahim, J. Frenzel, M. Frotscher, J. Pfetzing-Micklich, R. Steegmüller, M. Wohlschlögel, H. Mughrabi, G. Eggeler, Acta Mater. 61 (2013) 3667-3686.

[34] K. Gall, H.J. Maier, Acta Mater. 50 (2002) 4643-4657.

[35] A. Ahadi, Q. Sun, Acta Mater. 90 (2015) 272-281.

[36] J. Chen, H. Yin, Q. Sun, Acta Mater. 195 (2020) 141-150.

[37] X. Wang, S. Kustov, K. Li, D. Schryvers, B. Verlinden, J. Van Humbeeck, Acta Mater. 82 (2015) 224-233.

[38] Y. Kaynak, H. Tobe, R.D. Noebe, H.E. Karaca, I.S. Jawahir, Scripta Mater. 74 (2014) 60-63.

[39] W.-N. Hsu, E. Polatidis, M. Smid, N. Casati, S. Van Petegem, H. Van Swygenhoven, Acta Mater. 144 (2018) 874-883.

[40] J. Arghavani, F. Auricchio, R. Naghdabadi, A. Reali, S. Sohrabpour, Int. J. Plast. 26 (2010) 976-991.

[41] A. Ahadi, Q. Sun, Acta Mater. 76 (2014) 186-197.

[42] R.R. Adharapurapu, F. Jiang, K.S. Vecchio, G.T. Gray III, Acta Mater. 54 (2006) 4609-4620.

[43] S. Nemat-Nasser, J.Y. Choi, Acta Mater. 53 (2005) 449-454.

[44] G. Tan, Y. Liu, P. Sittner, M. Saunders, Scripta Mater. 50 (2004) 193-198.

[45] J.A. Shaw, S. Kyriakides, Acta Mater. 45 (1997) 683-700.

[46] P.K. Kumar, D.C. Lagoudas, Acta Mater. 58 (2010) 1618-1628.

[47] X. Huang, Y. Liu, Scripta Mater. 45 (2001) 153-160.

[48] S. Kustov, D. Salas, E. Cesari, R. Santamarta, J. Van Humbeeck, Acta Mater. 60(6-7) (2012) 2578-2592.

[49] Y. Song, M. Jin, X. Han, X. Wang, P. Chen, X. Jin, Acta Mater. 205 (2021) 116541.

[50] X. Wang, C. Li, B. Verlinden, J. Van Humbeeck, Scripta Mater. 69 (2013) 545-548.

[51] X. Wang, Z. Pu, Q. Yang, S. Huang, Z. Wang, S. Kustov, J. Van Humbeeck, Scripta Mater. 163 (2019) 57-61.

[52] Y. Sutou, T. Omori, K. Yamauchi, N. Ono, R. Kainuma, K. Ishida, Acta Mater. 53 (2005) 4121-4133.

[53] S. Alkan, H. Sehitoglu, Acta Mater. 175 (2019) 182-195.

[54] P. Sedmak, J. Pilch, L. Heller, J. Kopecek, J. Wright, P. Sedlak, M. Frost, P. Sittner, Science 353 (2016) 559-562.

[55] J.A. Shaw, S. Kyriakides, Int. J. Plast. 13 (1998) 837-871.

Declaration of interests

☒ The authors declare that they have no known competing financial interests or personal relationships that could have appeared to influence the work reported in this paper.

☐The authors declare the following financial interests/personal relationships which may be considered as potential competing interests:

Cover letter

Dear Editor,

Thank you very much for your editorial work with our submission (**SMM-21-0686**) entitled "**Anomalous stress-strain behavior of NiTi shape memory alloy close to the border of superelastic window**". This manuscript is the revised version of the submission.

Based on the reviewers' suggestions, we made some changes in our revised manuscript. The changes are highlighted with yellow background (black text on yellow). The detailed response to the reviewers' suggestions is shown in "Response to reviewers' comments".

Yours sincerely,

Xiebin Wang

(On behalf of all co-authors)

Figure-1

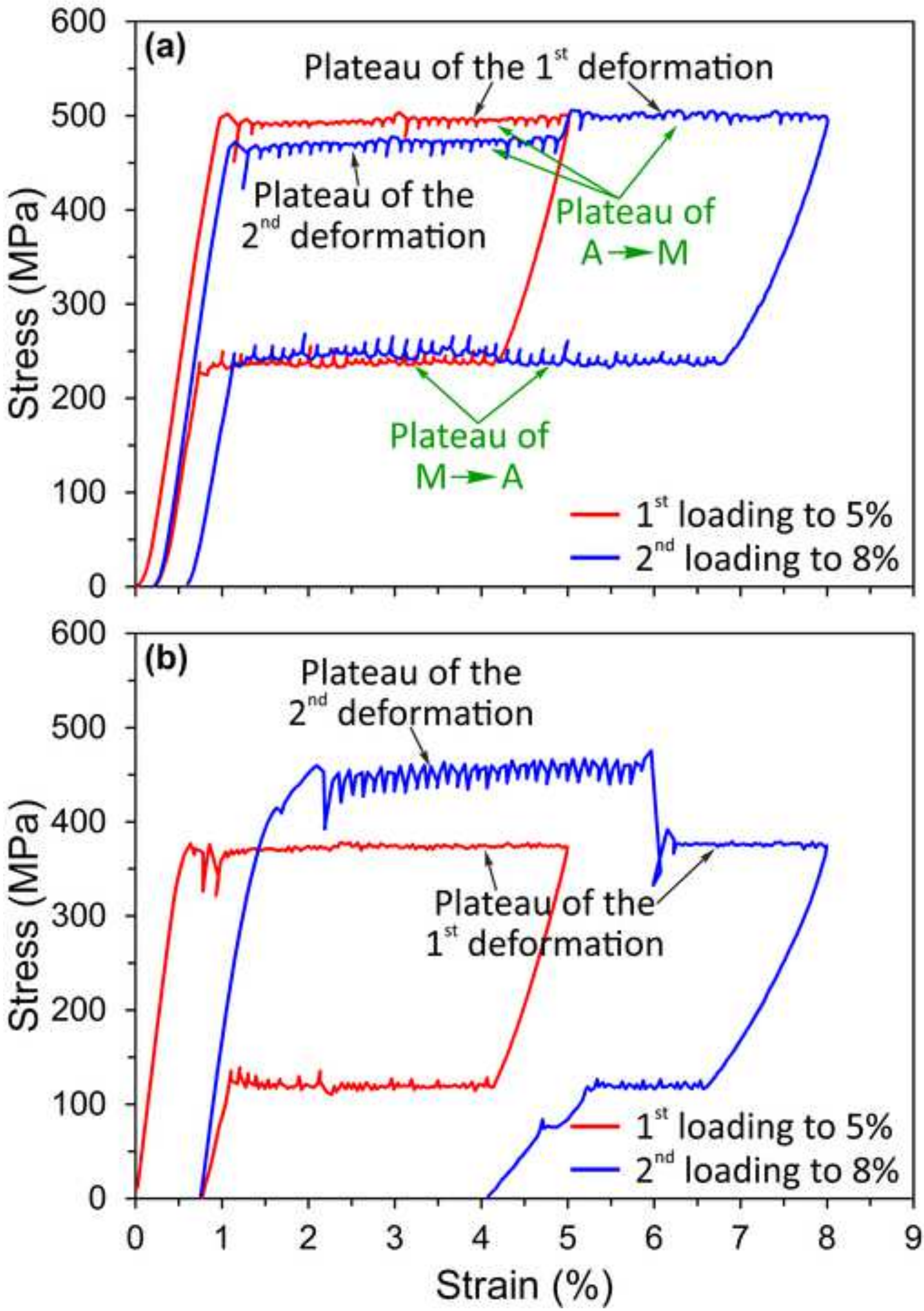
(a)
Plateau of the 1st deformation
Plateau of the 2nd deformation
Plateau of A→M
Plateau of M→A
1st loading to 5%
2nd loading to 8%
(b)
Plateau of the 2nd deformation
Plateau of the 1st deformation
1st loading to 5%
2nd loading to 8%
Stress (MPa)
Strain (%)
0
100
200
300
400
500
600
0
1
2
3
4
5
6
7
8
9

Figure-2

Click here to access/download;Figure(s);FIG-2.tif

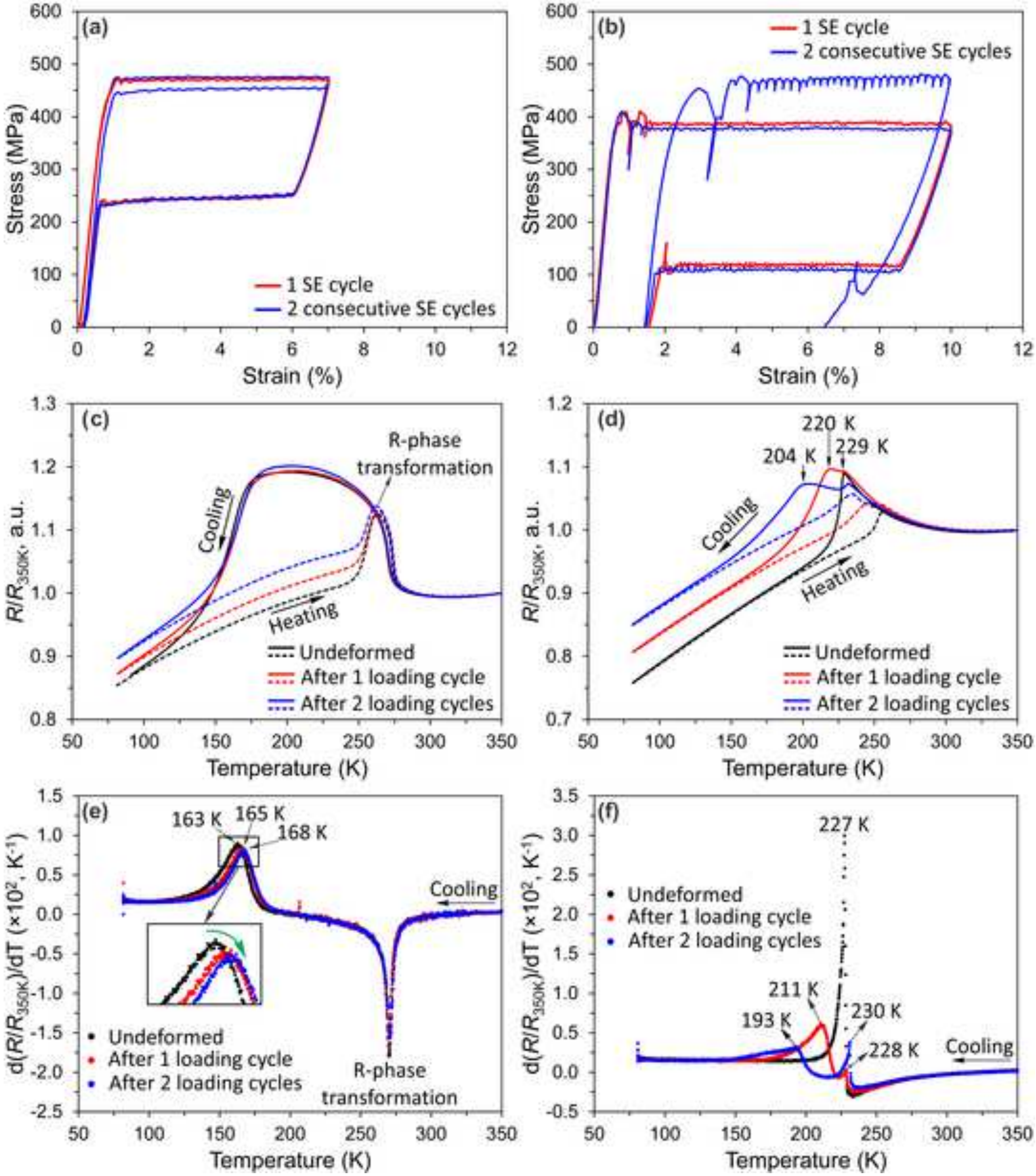

Figure-3

Click here to access/download;Figure(s);FIG-3.tif

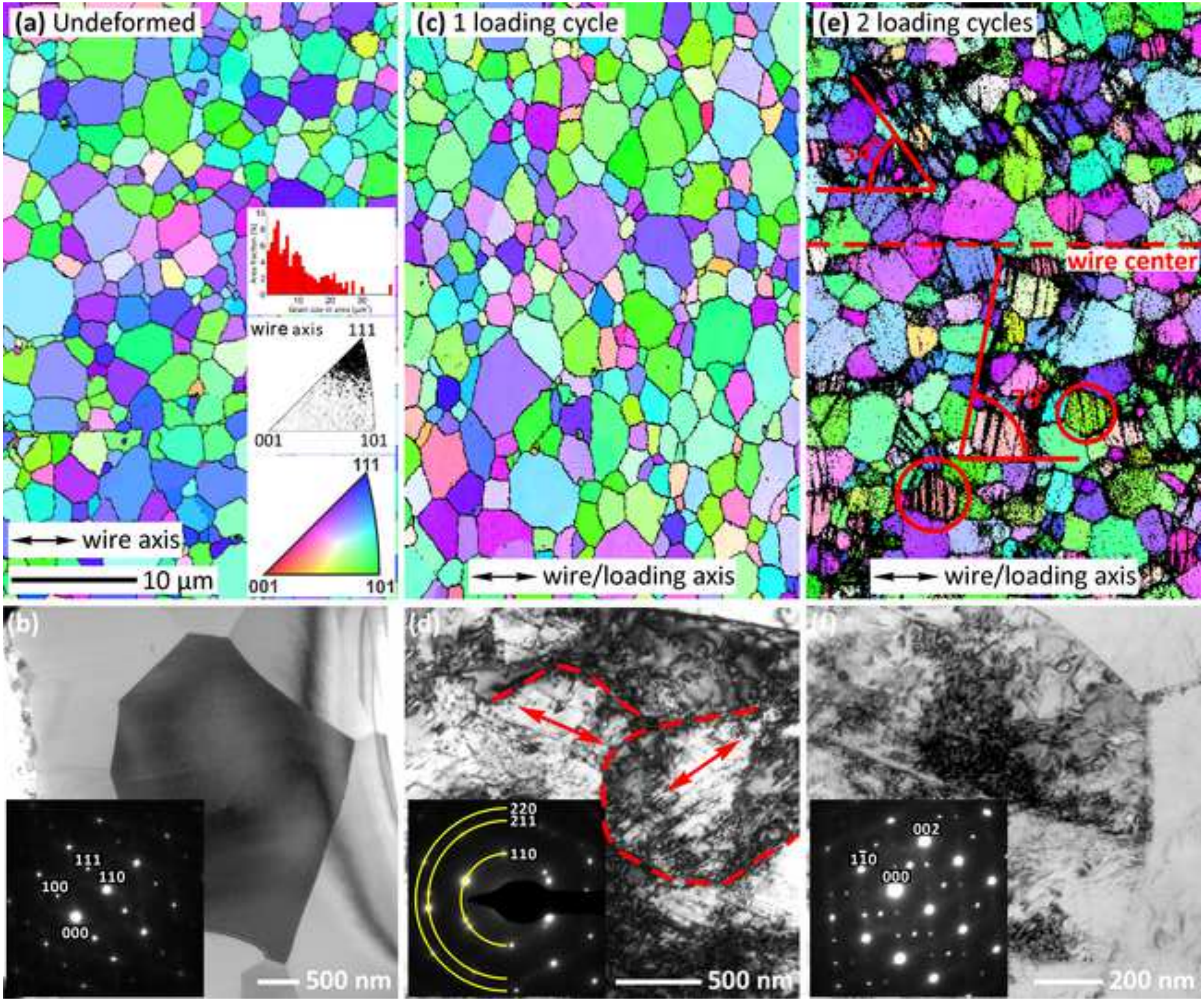

Figure-4

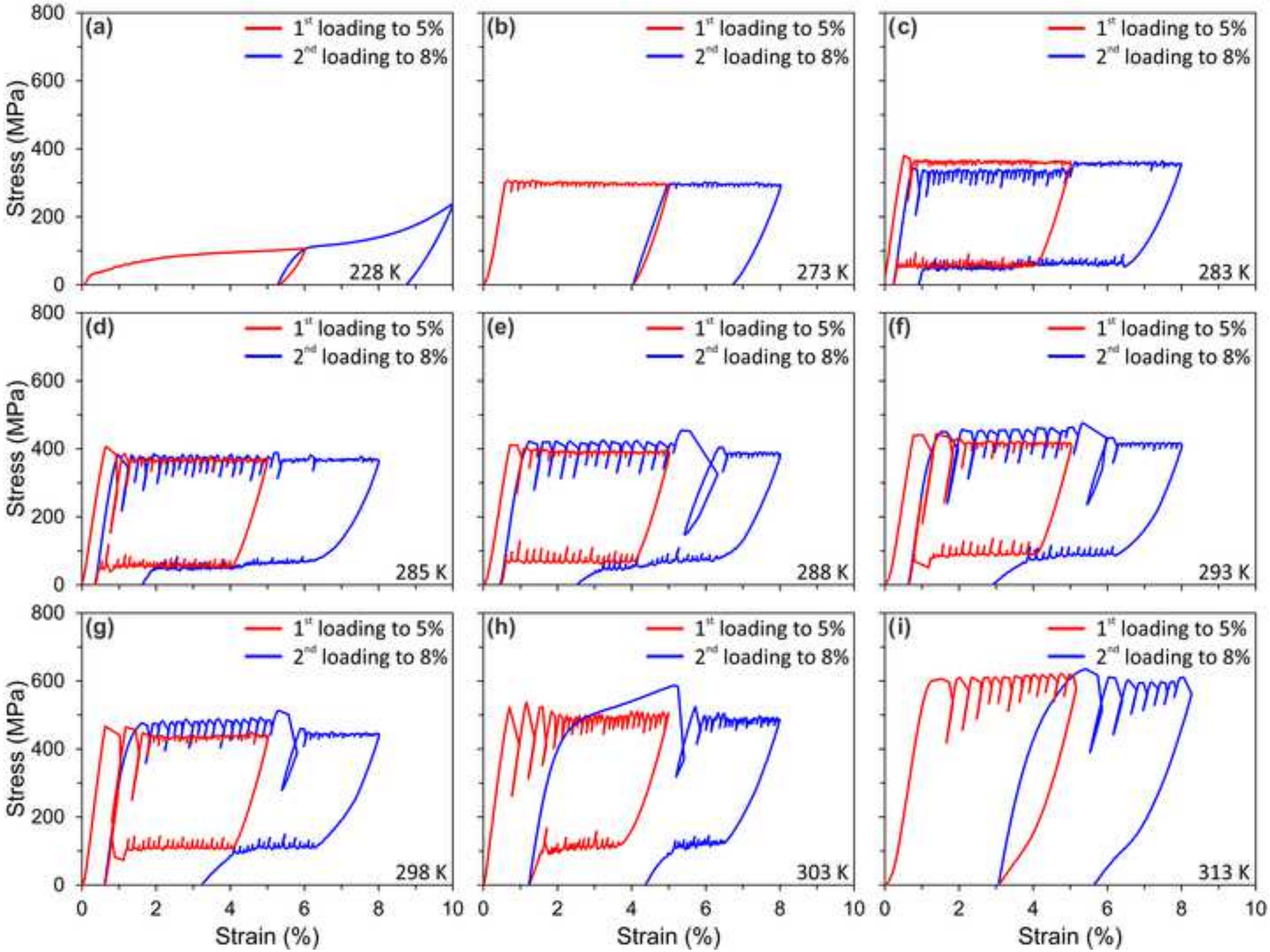

(a)
(b)
(c)
(d)
(e)
(f)
(g)
(h)
(i)
1st loading to 5%
2nd loading to 8%
228 K
273 K
283 K
285 K
288 K
293 K
298 K
303 K
313 K
Stress (MPa)
Strain (%)
0
200
400
600
800
0
2
4
6
8
10

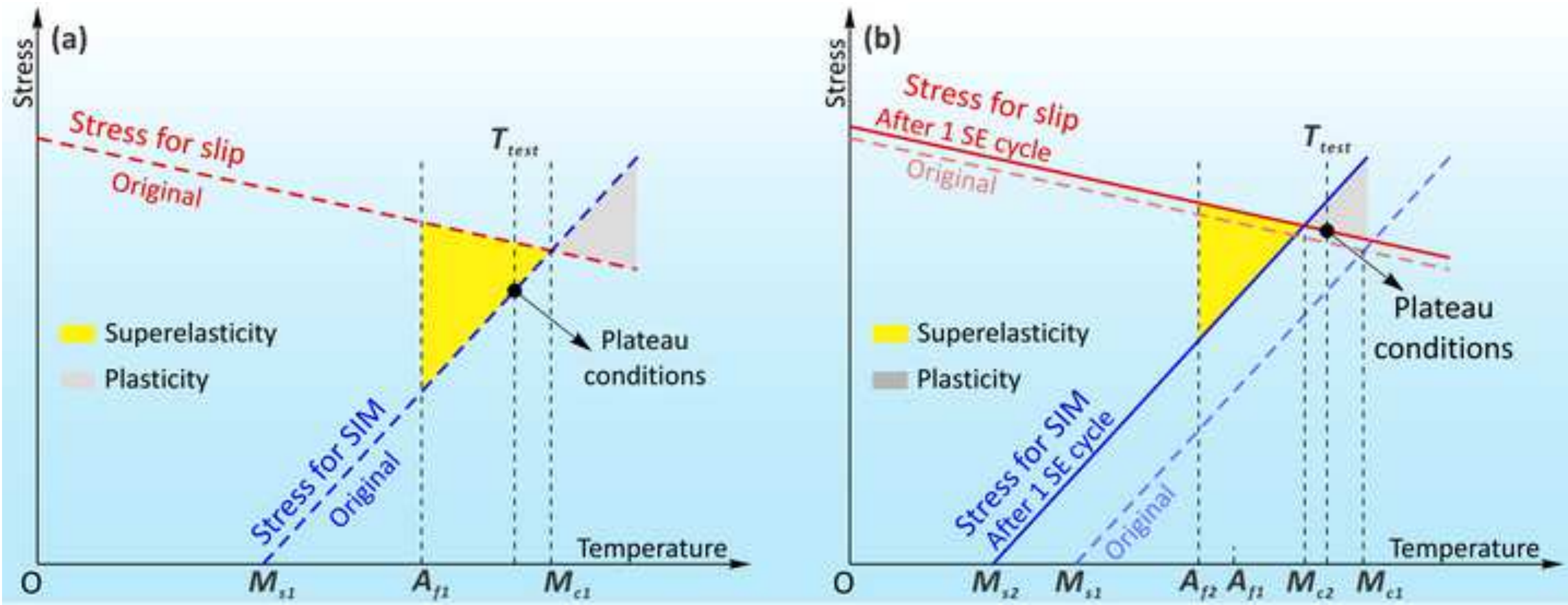
(a)
Stress
Stress for slip
Original
T test
Superelasticity
Plasticity
Plateau conditions
Stress for SIM
Original
Temperature
O
Ms1
Af1
Mc1
(b)
Stress
Stress for slip
After 1 SE cycle
Original
T test
Superelasticity
Plasticity
Plateau conditions
Stress for SIM
After 1 SE cycle
Original
Temperature
O
Ms2
Ms1
Af2
Af1
Mc2
Mc1